International Journal of Modern Physics C
Vol. 26, No. 8 (2015) 1550087 (14 pages)

DOI: 10.1142/S0129183115500874

Rarefied gas flow behavior in micro/nanochannels under specified wall heat flux

Mojtaba Balaj, Hassan Akhlaghi and Ehsan Roohi*

High Performance Computing (HPC) Laboratory
Department of Mechanical Engineering
Ferdowsi University of Mashhad
P.O. Box 91775-1111, Mashhad, Iran
**e.roohi@ferdowsi.um.ac.ir*

Received 5 September 2014
Accepted 20 November 2014
Published 2 January 2015

In this paper, we investigate the effects of convective heat transfer on the argon gas flow through micro/nanochannels subject to uniform wall heat flux (UWH) boundary condition using the direct simulation Monte Carlo (DSMC) method. Both the hot wall ($q_{\text{wall}} > 0$) and the cold wall ($q_{\text{wall}} < 0$) cases are considered. We consider the effect of wall heat flux on the centerline pressure, velocity profile and mass flow rate through the channel in the slip regime. The effects of rarefaction, property variations and compressibility are considered. We show that UWH boundary condition leads to the thermal transpiration. Our investigations showed that this thermal transpiration enhances the heat transfer rate at the walls in the case of hot walls and decreases it where the walls are being cooled. We also show that the deviation of the centerline pressure distribution from the linear distribution depends on the direction of the wall heat flux.

Keywords: Micro/nano channel; DSMC; constant wall heat flux boundary condition; iterative technique; thermal transpiration.

1. Introduction

Nowadays fabrications of small size channels used in biosensors, micro heat exchangers and Micro/Nano-Electro-Mechanical-Systems (MEMS/NEMS) with a size of several micrometers have become possible.[1,2] For an efficient and economical design, trustful prediction of fluid and heat transfer behavior through micro/nano-devices is essential.

Convective heat transfer for rarefied gas through microchannel has been investigated by different researchers. Inman[3] analytically studied the slip flow under uniform wall temperature (UWT) and proposed an expression for the wall heat flux as a function of flow rarefaction. Miyamoto *et al.*[4] investigated heat transfer

*Corresponding author.

characteristics of the choked flows in small-scale channel. Hadjiconstantinou[5] used DSMC technique to investigate convective heat transfer in slip and transition regimes. He studied analytically the effect of shear work at the boundary through solution of the constant wall heat flux problem in the slip-flow regime and verified the results using DSMC. Colin *et al.*[6] evaluated the accuracy of a second-order flow model in rectangular microchannels. Myong *et al.*[7] studied convective heat transfer in a microtube using a mathematical method extended from the classical Graetz problem. They considered the effects of axial heat conduction and evaluated the Langmuir model for surface slip. Weng and Chen[8] studied analytically the natural convective gas flow through a long open-ended vertical microchannel with constant but not necessarily symmetric wall heat fluxes. Their results indicated that thermal creep effect decreases the maximum gas temperature and flow drag. Niazmand *et al.*[9] studied the key flow parameters such as the friction and heat transfer in an isoflux rectangular microchannel under heating condition. They indicated that thermal creep reduces the friction coefficient and slightly enhances the heat transfer rates. They also showed that thermal creep effects become more pronounced at lower Reynolds number. Niazmand and Rahimi[10] investigated the natural convection flow in an open-ended vertical microchannel with isothermal walls. They showed that even with constant wall temperature, streamwise temperature gradient and therefore thermal creep effects exist near the walls due to temperature jump boundary condition. They found that thermal creep contribution to the velocity slip becomes dominant close to the channel inlet and vanishes in the fully developed region. Yan *et al.*[11] studied the thermal transpiration effect on hydrogen gas multiscale flow behaviors using a DSMC-SPH coupled approach. They showed that when the thermal transpiration effect is in the same direction as the driven pressure, the velocity and the mass flow rate of the hydrogen flow increase. Ganguly *et al.*[12] discussed rarefied gas flows in the presence of thermal creep and heat conduction conditions. They showed that the significance of the rarefied thermal creep varies considerably depending on the temperature and pressure and may be negligible at high pressure and low-temperature gradient.

The authors previously examined the hydro/thermal behavior of rarefied gas flow through micro/nanochannel.[13–18] Akhlaghi *et al.*[13] proposed an "Iterative Technique" for applying a desired heat flux distribution over the wall. It is shown that pressure distribution of microscale Poiseuille flow may become less than the linear incompressible one for cooling condition. The effect of nonuniform wall temperature distribution on the mass flow rate and thermal behavior of rarefied gas was considered in Refs. 14–16. Moreover, the effects of gas-surface heat transfer in the presence of UWT distribution on the mass flow rate and heat flux behavior were studied in Refs. 16 and 17. Knudsen number and viscous dissipation effects on the Nusselt number behavior were studied in the slip and transitional flow regimes in Ref. 18.

Some qualitative observation on pressure and velocity changes due to wall heat transfer is captured in Ref. 17. However, the details of pressure, temperature and

velocity fields of the Poiseuille flow under gas-surface heat transfer are not covered in the past studies. Current work presents a detailed discussion on wall heat transfer effects on the hydro/thermal behavior of micro/nanoscale Poiseuille flow. Field variations of pressure, velocity and temperature under nonzero wall heat flux condition are investigated in detail here. The results are obtained for UWT and uniform wall heat flux (UWH) cases. Nonzero wall heat flux is generated using an inflow-surface temperature difference.

2. DSMC Method

Knudsen number (Kn) is defined as the ratio of the gas mean free path (λ) to the flow characteristic length (H):

$$\mathrm{Kn} = \lambda / H. \tag{1}$$

Because of decreasing in medium density in small size geometries, rarefaction of flow, characterized by the Knudsen number, has a significant impact on the flow field and heat transfer behavior. Direct Simulation Monte Carlo (DSMC) method is a particle method based on the kinetic theory for the simulation of dilute gases.[19] The method is carried out by modeling the gas flow using many independent simulated particles. These simulated particles are representatives of a large number of real gas molecules in the flow field. The time step in the DSMC method is chosen as small as the positional changes of particles, and their collisions could be decoupled during each time step. In order to implement the DSMC algorithm, the flow field must be divided into computational cells. The size of each cell should be small enough to result in small changes in thermodynamic properties across each cell. The cells provide geometric boundaries and volumes, required to sample macroscopic properties. They are also used as a unit where only particles located within the same cell at a given time are allowed for collision. The cells are then typically divided into subcells in each direction. Subcells are utilized to decrease the collision separation distance between the collision pairs.

In the current study, the variable hard sphere (VHS) collision model is used to consider accurate variations of the viscosity with temperature. Based on this model, the mean free path of the gas is defined as follows[19]:

$$\lambda = \frac{2}{15}(5 - 2\omega)(7 - 2\omega)\sqrt{\frac{m}{2\pi\kappa T}}\left(\frac{\mu}{\rho}\right), \tag{2}$$

where ω, m, κ, T, μ and ρ are viscosity-temperature index, gas mass, Boltzmann constant, gas temperature, gas viscosity and density, respectively. Dependency of the VHS gas viscosity on the bulk temperature is computed according to Ref. 19:

$$\mu = \frac{15m}{8\Gamma(4 - v)} \frac{(\pi RT)^{0.5}(4RT)^{v}}{\sigma c_r^{2v}}, \tag{3}$$

where c_r is the relative speed of collision pairs, v is a constant in the range 0 to 0.5 and $\sigma = \pi d^2$ is the total collision cross-section. The gas constant is given by $R = \kappa/m$. d is the molecular diameter and calculated as follows:

$$d = d_{\text{ref}} \left(\frac{\left(\frac{2\kappa T_{\text{ref}}}{m_r c_r^2}\right)^{\omega-0.5}}{\Gamma(2.5-\omega)} \right)^{0.5}, \tag{4}$$

where Γ is the gamma function and m_{r} is the reduced mass of collision pairs, and the ref index indicates the reference parameters. For argon gas flow, Macrossan[20] suggested that an accurate variation of the viscosity with temperature could be obtained with $v = 1/6$. The choice of collision pair is done based on the No Time Counter (NTC) method.

Temperature jump in the DSMC method is calculated based on the direct microscopic sampling from the corresponding particle properties which strike the wall surface as follows[21]:

$$T_j - T_w = \frac{1}{3R} \frac{\sum \left(\frac{1}{|v_p|} U_P^2\right) - \sum \left(\frac{1}{|v_p|}\right) u_{\text{slip}}^2}{\sum \left(\frac{1}{|v_p|}\right)}, \tag{5}$$

where p index indicates particle, $|v_p|$ is the absolute value of the normal velocity, U_P is the velocity magnitude and u_{slip} is the slip velocity at the wall obtained according to the following formula:

$$u_{\text{slip}} = \frac{\sum \left(\frac{m}{|v_p|} u_p\right)}{\sum \left(\frac{m}{|v_p|}\right)}. \tag{6}$$

Also the bulk temperature (T_b) is defined as:

$$T_b = \frac{\int_A \rho u_x T dA}{\int_A \rho u_x dA}. \tag{7}$$

Monatomic argon is considered as the working fluid. In order to ensure the satisfaction of the limits on the cell size, the cell dimensions are considered as 0.1 λ and are much smaller than that for most cases. All walls are treated as diffuse reflectors using the full thermal accommodation coefficient. Half-range Maxwellian distribution is used to determine the velocity of the wall-reflected particles. After achieving steady flow condition, sampling of flow properties within each cell is fulfilled during a sufficient period to suppress the statistical scatters of the solution. All thermodynamic parameters such as velocity, density, and temperature are then determined from this time-averaged data. Inlet/outlet pressure boundary conditions are imposed according to the formula proposed by Wang and Li.[22] The specified wall heat flux distribution is imposed via Iterative Technique.[13] It is useful to present the magnitude of different wall heat fluxes in the nondimensional form. We employ the reduced wall

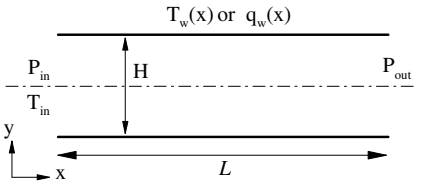

Fig. 1. Micro/nanochannel geometry and imposed boundary conditions.

heat flux parameter (q^*) which is defined based on the Stanton number in Ref. 16.

$$q^* = \frac{q_w L}{\dot{m} C_p T_{\text{avg}}}, \tag{8}$$

where $\dot{m}$ is the channel mass flow rate, C_p is the specific heat, T_{avg} is the average temperature and L is the channel length. To investigate the numerical convergence and accuracy, we compare our computed distribution of the pressure with the analytical solution of Ref. 23 for the Poiseuille flow under constant temperature wall condition. Figure 1 shows the geometry of the micro/nano channel and imposed boundary conditions.

Figure 2 shows the effect of DSMC time step, numbers of simulator particles per cell (N_{PPC}), and simulation time on the pressure distribution along the channel. The results are compared with the analytical solution based on the second-order accurate slip boundary condition given in Ref. 23. Lines in Fig. 2(a) correspond to DSMC time steps equal to 0.08, 0.16 and 1.6 mean collision time, respectively. According to this figure, expect the large disagreements in the case of $(\delta t/\delta t_\lambda)_{\max} = 1.6$, other values of employed time steps predict the pressure distribution along the channel suitably. Figure 2(b) shows the effect of N_{PPC} on the pressure distribution along the channel. The results indicate that the values of N_{PPC} equal to 20 and 40 are reliable for continuing the calculations. Figure 2(c) describes the pressure distribution evolution during the simulation. The flow and wall sampling period are set equal to $5 \times 10^4\ \delta t$. It is observed that the pressure distribution converges with time and the final distribution has been attained at $t = 2 \times 10^6\ \delta t$.

3. Results and Discussion

3.1. *Effects of the channel aspect ratio (AR)*

Figure 3 investigates the effects of channel aspect ratio on different axial and cross-sectional parameters. In this investigation, it is important to keep the reduced wall heat flux the same for all the channels with different aspect ratios. Here, it is set to be $q^* = -0.3$ for all cases. Figure 3(a) shows the velocity profile at a constant Knudsen number of $\text{Kn} = 0.06$. This figure shows that the dimensionless velocity profile is quite close for aspect ratio of 20 and 30 at a constant $\text{Kn} = 0.06$. Figures 3(b)–3(d) demonstrate that the sensitivity of Knudsen number, normalized bulk temperature and centerline pressure with respect to the channel aspect ratio. This figure indicates

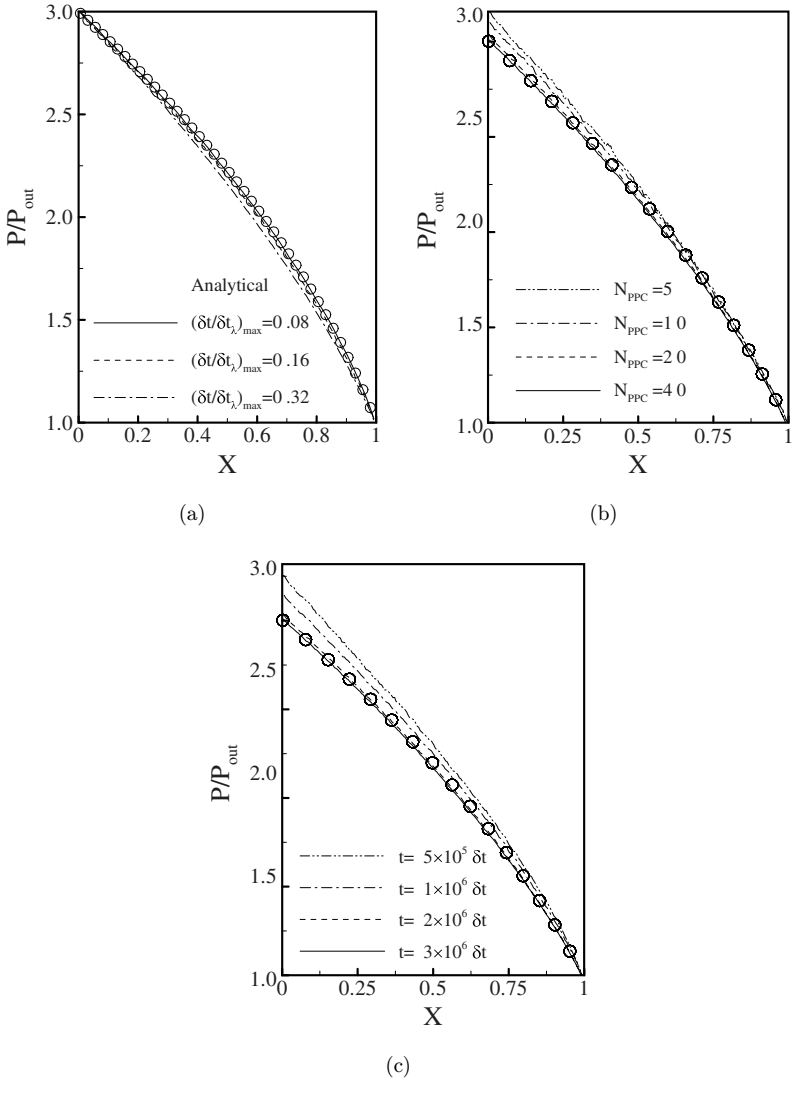

Fig. 2. Pressure distribution along the channel for different DSMC time step values (a), numbers of simulators (b) and simulation times at adiabatic condition ($q^* = 0$). (c) Centerline pressure distribution.

that the changes of the dimensionless parameters shown here are negligible for aspect ratio of 20 and 30. This observation is consistent with our previous experiences on the micro/nanochannel research where a constant unidirectional temperature gradient is applied to the walls.[14] We already showed that the DSMC results do not depend on the aspect ratio for AR $\geq$ 20 channels.[14] Therefore, to set a balance between the numerical cost and accuracy, we set the channel aspect ratio equal to 20. The pressure ratio (PR) is set equal to 3. Table 1 represents main parameters of

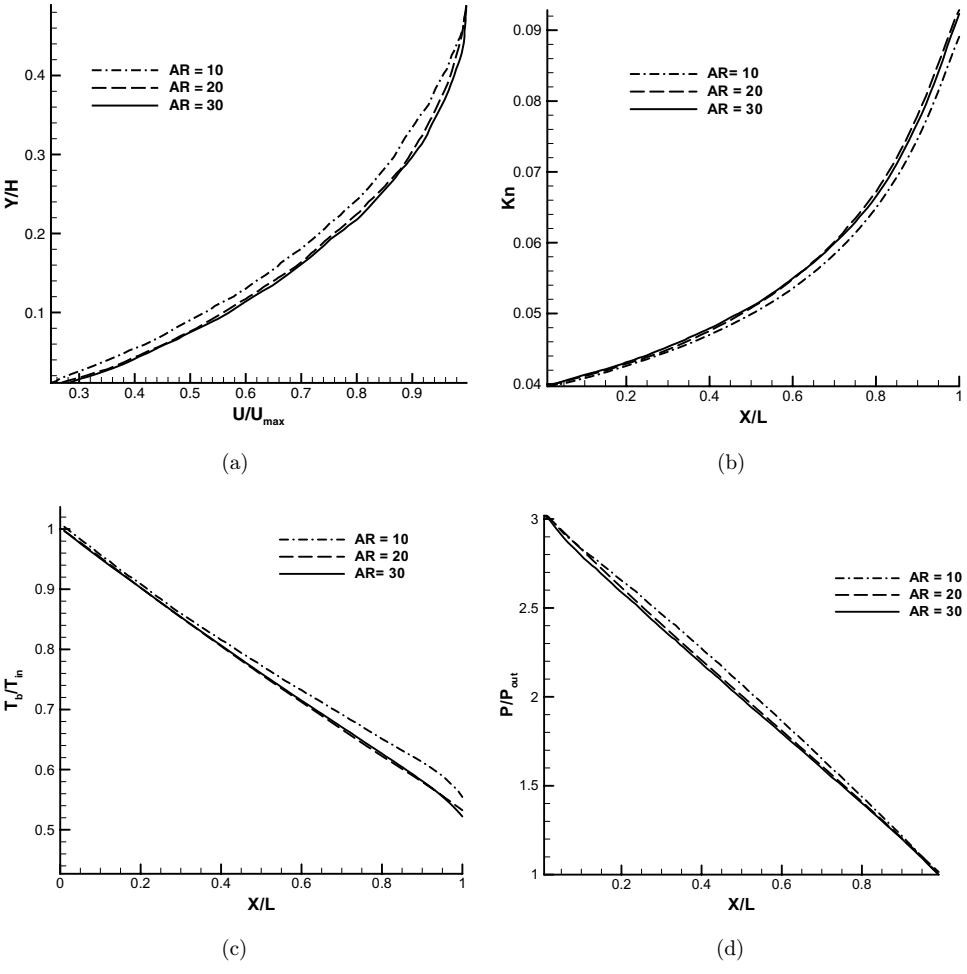

Fig. 3. (a) Velocity, (b) Knudsen number, (c) temperature, and (d) pressure variations along the channel in UWH case with $q^* = -0.3$ and different channel aspect ratios.

Table 1. The fundamental parameters of investigated cases with $\mathrm{Kn}_{\mathrm{avg}} = 0.045$.

Case number	Wall B.C.	$\mathrm{Kn}_{\mathrm{in}}$	q^*
1	Cooling UWH	0.04	−0.4
2	Cooling UWH	0.04	−0.3
3	Cooling UWH	0.04	−0.2
4	Adiabatic UWH	0.03	0.0
5	Adiabatic UWT	0.03	0.0
6	Heating UWH	0.02	0.2
7	Heating UWH	0.02	0.3
8	Heating UWH	0.02	0.4

investigated cases. It should be noted the simulations were performed in channels with height in both micro and nano scales, i.e. height of 100 μm and 100 nm.

3.2. *Velocity profile*

There are wide sets of analytical solutions for pressure driven isothermal microchannel flows, i.e. see Ref. 24. In this section, we evaluate the suitability of these types of analytical solutions for flows under UWT and UWH boundary conditions. Then the effects of wall heat flux on the velocity profile will be discussed.

Figure 4 compares the analytical solution[24] with the current DSMC simulations for $q^* = 0.3$ (Case 2), $q^* = -0.3$ (Case 7) and $q^* = 0.0$ conditions (Case 5) at Kn = 0.09. The UWT case with $q^* = 0.0$ agrees with the analytical solution with an error of $\pm 5\%$, while constant wall heat flux simulations show more/less velocity slip relative to the analytical solution. As the figure shows, that heating increases the nondimensional slip velocity while cooling decreases it.

Figure 5 illustrates the dimensionless velocity profile from our simulations for different reduced wall heat flux for two Knudsen numbers of 0.045 and 0.08. The graph shows that slip velocity changes slightly once the reduced wall heat flux magnitude varies at a constant Kn. However, the effect of heat flux on the velocity is more pronounced at higher heat flux magnitude. Similar to Fig. 4, we conclude that heating increases the magnitude of nondimensional velocity slip and cooling decreases it. It is due to the thermal creep (transpiration) effects. Thermal creep effects produce an additional slip velocity, which directs the flow from the colder region toward the hotter region. In practice, thermal creep is the primary driving mechanism for Knudsen pumps.[25] It is observed that this additional slip velocity increases as soon as Kn increases. Cases of adiabatic wall and constant temperature

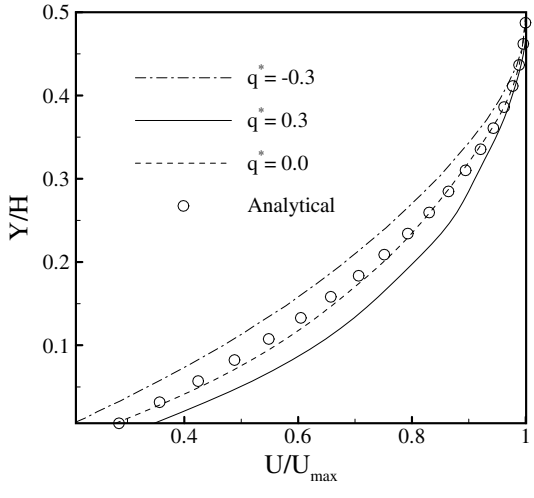

Fig. 4. Velocity profiles under different wall thermal conditions.

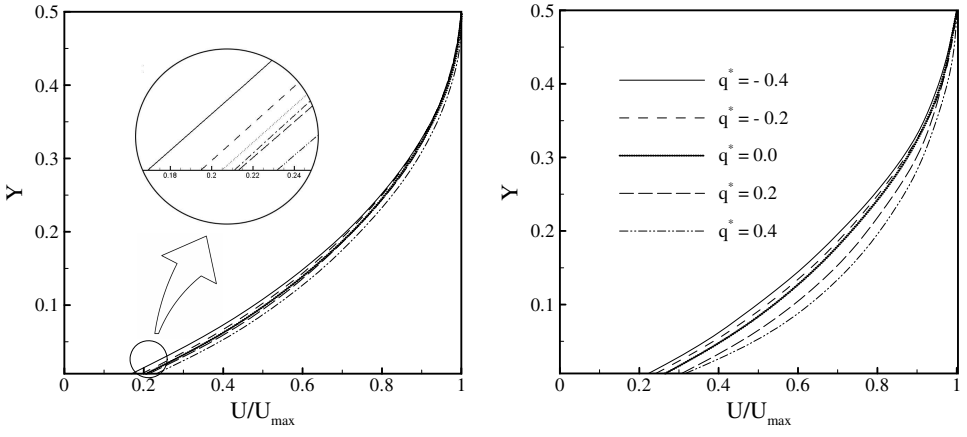

(a) Kn = 0.045 (b) Kn = 0.080

Fig. 5. Effect of wall heat flux on velocity profiles at different flow rarefactions in micro and nano channels. (a) Kn = 0.045, (b) Kn = 0.08.

wall show close behavior for the velocity profile. It is because the rate of heat transfer with the wall is almost negligible for constant temperature wall as the inlet temperature and wall temperature are close to each other. Hong and Asako[26] physically explained that when there is a slip, the shear work due to the slip at the wall acts as the heat flux in the form of $\mu u_s \, \partial u/\partial y$ from the wall. This term indicates that the effect of viscous dissipation always behaves like a heat source, i.e. heat generation made by the shear stress is usually considerable. The effect of the viscous dissipation depends on whether the walls are being cooled or heated. Conferring to Fig. 5, it could be concluded that the thermal creep in the case of hot walls enhances the heat transfer rate due to increased advection and thermal creep due to cold walls reduces it.

Thermal creep occurs when there is a temperature gradient in the flow near the walls. Now the question is how the temperature gradient in the flow is created. To impose a temperature gradient in the flow, we could specify a heat flux at the wall, which subsequently leads to a temperature gradient in the gas near the walls due to temperature jump condition, and hence thermal creep flow. Figure 5 indicates that the thermal creep can enhance or reduce the mass flow rate in a channel depending on the specified heat flux at the wall, i.e. the direction of the tangential temperature gradient of the channel wall.

3.3. *Temperature distribution*

Figure 6 shows variations of wall, jump and bulk temperature for the different q_w cases. This figure shows that heating wall flux imposes a positive temperature gradient along the channel while cooling wall flux leads to a decrease in the temperature.

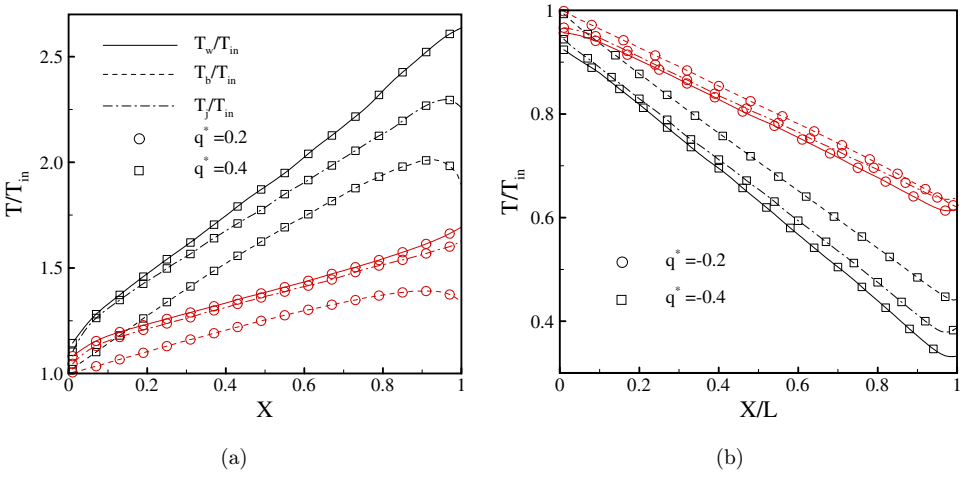

Fig. 6. (Color online) Variation of wall temperature (T_w), jump temperature (T_j) and bulk temperature (T_b) for different heating (a) and cooling (b) wall conditions.

Also, this figure illustrates the end expansion cooling effect, especially in the case of hot walls. It is observed that the difference of T_w and T_b and the temperature gradient in the flow, i.e. dT_b/dx and near the wall, i.e. dT_j/dx increases as the magnitude of reduced wall heat flux increases. For cold wall cases, the bulk temperature is greater than wall temperature, and vice versa. The primary driving mechanism for the heat transfer from the wall to the fluid is the temperature difference between the wall and the bulk fluid. According to Fig. 5 and Fig. 6, it could be concluded that the increase in the temperature gradient which is directly related to the specified heat flux at higher heat fluxes increases the thermal creep near the walls.

Figure 7 shows the dimensionless temperature and Kn contour fields for different q^* magnitudes. According to this figure, temperature increases along the channel for positive heat flux and decreases for negative wall heat flux. There is approximately no heat transfer in adiabatic wall case (Case 4). In this case, temperature decreases due to the flow acceleration along the channel. Additionally, the figure denotes that for all cases the flow rarefies along the channel due to flow acceleration and pressure drop. The energy transfer from the wall to the fluid causes a decrease in the gas density and flow rarefies more since the pressure ratio is kept constant along the channel. This means that the gas rarefaction increases with heat addition to the flow and vice versa.

3.4. *Pressure behavior*

The effect of different reduced wall heat flux on the centerline pressure distribution along the channel is now considered. We compare DSMC results for UWT channels

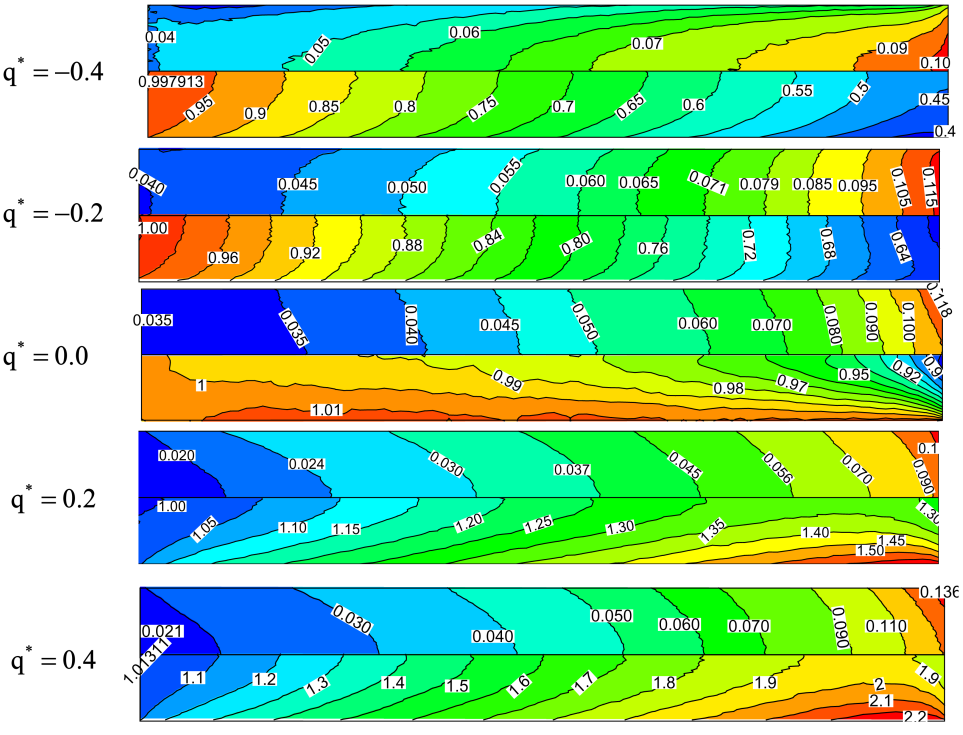

Fig. 7. (Color online) Temperature (lower) and Knudsen number (upper) fields for different values of q^*.

with a second-order accurate expression for centerline pressure distribution given in Ref. 23. Additionally, we would like to examine the pressure distribution of UWT channels with those of UWH channels. To consider this, we expose the channel to two different reduced wall heat flux equal to -0.3 and 0.3 (Case 2 and Case 7) for both cooling and heating conditions, as shown in Fig. 8. This figure shows the pressure distribution for a microchannel subject to UWH (Case 2 and Case 7) and UWT (Case 5) boundary conditions. According to Fig. 8, the current DSMC simulations for UWT case agree well with the analytical solution and the differences are less than 6% relative to the analytical solution. Figure 8 shows that the UWH solutions are different from the analytical solution. Heating increases the compressibility of the fluid and produces positive curvature while cooling decreases density variations and produces negative curvature.

Figure 9 shows the centerline pressure under UWT and UWH wall conditions for the same pressure ratio and inlet condition ($P_{\text{in}} = 100\,\text{kPa}$). Considering these, curvature of the pressure distribution increases as soon as the reduced wall heat flux increases. This increase is more pronounced at higher reduced wall heat flux magnitudes, i.e. compare two cases with $q^* = 0.2$ (Case 6) and $q^* = 0.4$ (Case 8). The figure also shows that the pressure distribution deviates from UWT (Case 5) as the magnitude of reduced wall heat flux increases, for both cooling and heating

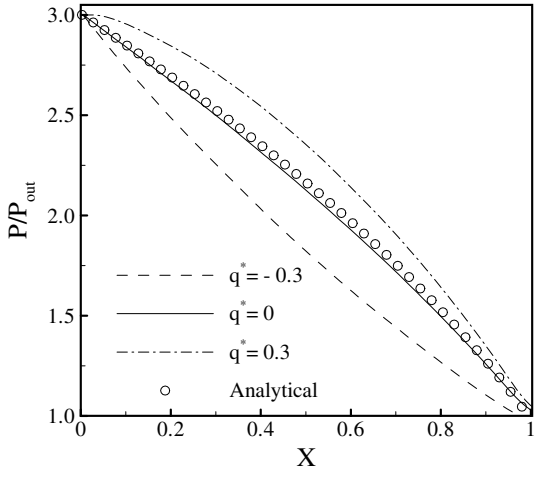

Fig. 8. Pressure distribution for different wall heat flux magnitudes.

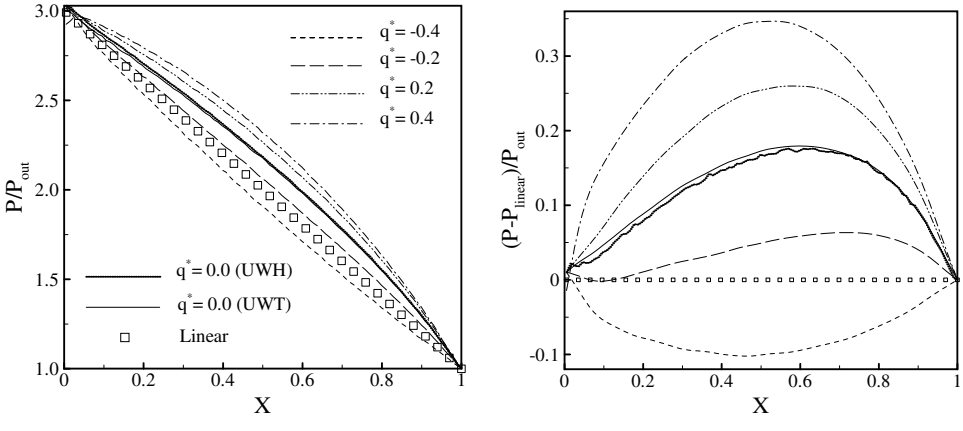

Fig. 9. Pressure distributions compared with linear distribution under different UWH conditions.

conditions. Based on the analytical solution, pressure distribution strongly depends on the exit flow average Knudsen number, i.e. the pressure distribution deviation from the linear distribution increases as the exit average Knudsen number increases. In comparison with the UWT case, the wall heat flux leads to an increase or a decrease in the exit Knudsen number. It depends on that whether boundary condition is cooling or heating, i.e. in cooling cases; the exit Knudsen number decreases in comparison to UWT case.

4. Conclusions

The convective heat transfer of argon gas flow in the slip regime through a parallel plate micro/nano channel with the specified reduced wall heat flux has been

investigated using the DSMC technique. Our investigation covered both of the hot wall ($q^* > 0$) and the cold wall ($q^* < 0$) cases. The effect of wall heat transfer on the velocity slip and centerline pressure distributions along the channel is discussed. We found that the thermal creep enhances the rarefaction effects under heating wall boundary condition, i.e. heating increases the velocity slip while cooling decreases it. It is consistent with the first-order Maxwell slip boundary condition which connects velocity slip to the velocity gradient and thermal creep effects. We also found that wall temperature differs more from the bulk temperature as Knudsen number increases. It may be due to the hindering of information propagation due to the enhanced flow rarefaction. The curvature of the centerline pressure distribution increased with the wall heat flux. This increase is more pronounced at higher reduced wall heat flux magnitudes. The high cooling heat flux may lead to a negative curvature in the centerline pressure distribution.

References

1. S. Prakash, M. Pinti and B. Bhushan, *Philos. Trans. R. Soc. A* **370**, 2269 (2012).
2. M. Pinti, T. Kambham, B. Wang and S. Prakash, *J. Nanotechnol. Eng. Med.* **4**, 021003-1 (2013).
3. R. Inman, Laminar slip flow heat transfer in a parallel plate channel or a round tube with uniform wall heating, NASA Technical Note D-2393 (1964).
4. M. Miyamoto, W. Shi, Y. Katoh and J. Kurima, *Int. J. Heat Mass Transf.* **46**, 2685 (2003).
5. N. G. Hadjiconstantinou, *J. Heat Transf.* **125**, 944 (2003).
6. S. Colin, P. Lalonde and R. Caen, *Heat Transf. Eng.* **25**, 23 (2004).
7. R. S. Myong, D. A. Lockerby and J. M. Reese, *Int. J. Heat Mass Transf.* **49**, 2502 (2006).
8. H. Chu Weng and C. Chen, *J. Phys. D: Appl. Phys.* **41**, 115501 (2008).
9. H. Niazmand, A. Amiri Jaghargh and M. Renksizbulut, *J. Appl. Fluid Mech.* **3**, 33 (2010).
10. H. Niazmand and B. Rahimi, High order slip and thermal creep effects in micro channel natural convection, in *ASME 2010 8th Int. Conf. Nanochannels, Microchannels, and Minichannels Collocated with 3rd Joint US-European Fluids Engineering Summer Meeting*, FEDSM-ICNMM2010-30688, ASME (American Society of Mechanical Engineering).
11. J. Ye, J. Yang, J. Zheng, X. Ding, I. Wong, W. Li and C. Chen, *Int. J. Hydrog. Energy* **37**, 12474 (2012).
12. A. Ganguly, S. L. Nail and A. A. Alexeenko, *Vacuum* **86**, 1739 (2012).
13. H. Akhlaghi, E. Roohi and S. Stefanov, *Int. J. Thermal Sci.* **59**, 111 (2012).
14. H. Akhlaghi, M. Balaj and E. Roohi, *Appl. Phys. Lett.* **103**, 073108 (2013).
15. H. Akhlaghi and E. Roohi, *Contin. Mech. Thermodyn.* **26**, 67 (2014).
16. H. Akhlaghi, E. Roohi and M. Balaj, *Appl. Phys. Lett.* **104**, 073109 (2014).
17. H. Akhlaghi, E. Roohi and M. Balaj, *Phys. Fluids* **26**, 092002-11 (2014).
18. M. Balaj, E. Roohi, H. Akhlaghi and R. S. Myong, *Int. J. Heat Mass Transf.* **71**, 633 (2014).
19. G. A. Bird, *Molecular Gas Dynamics and the Direct Simulation of Gas Flows* (Oxford Science, Oxford, U.K., 1994).
20. M. N. Macrossan, *J. Comput. Phys.* **185**, 612 (2003).
21. A. J. Lofthouse, Ph.D. thesis, University of Michigan (2008).
22. M. Wang and Z. Li, *Int. J. Heat Fluid Flow* **25**, 975 (2004).

23. N. Dongari, A. Agrawal and A. Agrawal, *Int. J. Heat Mass Transf.* **50**, 3411 (2007).
24. G. Karniadakis, A. Beskok and N. Aluru, *Microflows and Nanoflows: Fundamentals and Simulation* (Springer Science, 2005).
25. N. K. Gupta and Y. B. Gianchandani, *Journal of Micromech. Microeng.* **21**, 095029 (2011).
26. C. Hong and Y. Asako, *Int. J. Heat Mass Transf.* **53**, 3075 (2010).